

Path Planning for Planetary Exploration Rovers and Its Evaluation Based on Wheel Slip Dynamics

Genya Ishigami, Keiji Nagatani, and Kazuya Yoshida

Abstract—In this paper, a path planning and its evaluation method is described with paying attention to wheel slip dynamics of lunar/planetary exploration rovers. The surface of the planetary body is mostly covered with powdery soil. On such loose soil, wheel slippage that will make the rover get stuck or tip over must be concerned. Since the slippage dynamically depends on postures and velocities of wheel/vehicle and also soil characteristics, it is difficult problem to explicitly include the wheel slip dynamics as a criterion into path-planning algorithms. To tackle the slippage problem, the authors have developed a path-planning algorithm and a path-evaluation method based on wheel slip dynamics. In our approach, first, a path on rough terrain is simply generated with terrain-based criteria function. Then, the planned path is directly plugged into the dynamics simulation and the rover in the simulation travels along with the path. Finally, the path is properly evaluated based on slip motion profiles calculated by the simulation. Examples of the proposed technique are demonstrated with discussing characteristics of planned path and the slip motion profile of the rover.

I. INTRODUCTION

Substantial progresses in space exploration technology have significantly enabled us to perform various scientific missions, such as investigations about the origin of the solar system and the future in-situ resource utilization. Surface mobility is an important technology to expand exploration areas and deliver the in-situ devices to specific locations. The effectiveness of wheeled mobile robots (*Rovers*) in such missions has been demonstrated by both of NASA's Spirit and Opportunity rovers since 2004 [1]. Because of growing demand for more complex missions, rovers are expected to travel much longer distances, climb hills and traverse slopes.

The surface of the planetary body, such as the Moon or Mars, is covered with fine granular soil, boulders, rocks or stones spread over the terrain. On such challenging terrain, the rover must design the safest path to avoid mobility hazards such as wheel stuck, vehicle tip over and collision with obstacles.

There are a great number of papers and books regarding path/motion planning issues [2]-[7]. For example, Shiller et al. investigated a dynamic motion planning considering constraints on vehicle motions, such as sliding, tip over and velocity limit curves [3]. Howard et al. also proposed a fairly general constrained optimization approach to trajectory generation [5]. Iagnemma et al. developed a planning algorithm with model-based evaluation which takes into account

uncertainties of terrain measurements and rover localizations [6]. Most of these researches, however, have not explicitly included slip dynamics. Though general cruising velocity of the rover is relatively slow, the slip motion is easily generated when the rover travels on loose terrain. Since the slip motion dynamically depends on the posture of a rover, velocities of its wheels and soil or terrain characteristics, it is difficult problem to explicitly include the slip dynamics as a criterion into path-planning algorithms.

The mechanics of a slipping wheel on loose soil has been studied in the field of *Terramechanics* [8]-[11]. In this field, analysis of wheel-soil interaction mechanisms and modeling of stress distributions underneath a wheel on loose soil have been well investigated [8][9]. The authors have also previously elaborated the wheel-and-vehicle model to deal with traveling characteristics of rovers [10][11].

In this paper, applying our background regarding wheel slip dynamics, a path planning algorithm and its evaluation method is addressed to deal with the slippage problems. Our approach consists of three steps: the first step is a path planning from a start position to a destination on rough terrain. The path-planning problem is addressed as an extended shortest path problem and the conventional Dijkstra's algorithm is employed to find a candidate path. Then, as the second step, the planned path is directly plugged into the dynamics simulation elaborated in our previous research. The rover in the simulation is controlled to follow the given path. Finally, in the third step, the path is properly evaluated based on the results of the dynamics simulation. The criteria of the path evaluation are defined as wheel slippages and vehicle postures.

Examples of the proposed technique are demonstrated and the result shows that the proposed technique is able to quantitatively evaluate and discuss which path are slip less, hazard less, and the safest.

The paper is organized as follows: Section II describes an outline of the proposed technique for the path planning and the evaluation method. In Section III, the path-planning algorithm is introduced. The dynamics simulation model and the path following strategy for the path evaluation method are presented in Section IV and Section V, respectively. In Section VI, the simulation study and performance of the proposed technique are described.

II. OUTLINE OF PATH PLANNING AND EVALUATION METHOD

In this section, the outline of the proposed technique for path planning and its evaluation method is described. Fig. 1

This work was supported in part by Research Fellowships of the Japan Society for the Promotion of Science for Young Scientists.

The authors are with Department of Aerospace Engineering, Tohoku University, Aoba 6-6-01, Sendai, 980-8579, Japan, {ishigami, keiji, yoshida}@astro.mech.tohoku.ac.jp

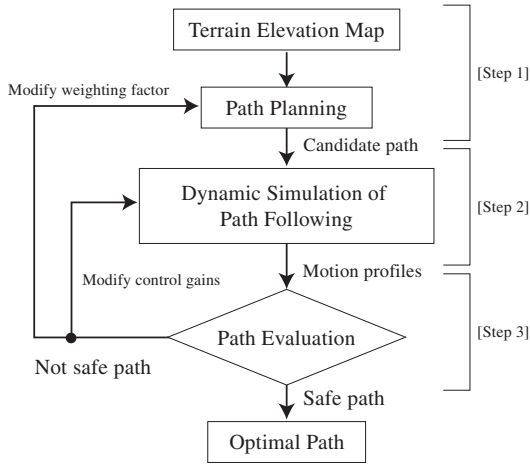


Fig. 1. Flow chart of the path planning algorithm and evaluation method

shows a flow chart of the proposed technique.

As mentioned above, our approach consists of three steps: 1) path planning to find a candidate path, 2) dynamics simulation to follow the planned path, and 3) path evaluation based on the dynamic simulation results.

In the first step, the path-planning problem is addressed as an extended shortest path problem and a candidate path is found based on the conventional Dijkstra's algorithm [7].

As the second step, the dynamics simulation of path following is carried out to calculate motion profiles of the rover when the rover is controlled to follow the planned path. It is possible to take into account the path-following error since the rover might not accurately follow the desired path. In the simulation, the dynamic behavior of a rover is modeled with the wheel-and-vehicle model, which has been developed and validated in our previous research [10][11]. The interaction of wheel on loose soil is properly addressed based on the terramechanics approach.

Then in the third step, the path is properly evaluated based on the results of the dynamic simulation. The criteria of the path evaluation are determined as wheel slip dynamics, vehicle postures and elapsed time/total traveling distance to reach the destination.

III. PATH PLANNING ALGORITHM

The path-planning algorithm addressed in this section derives a certain path based on a criteria function. To find a candidate path, the path-planning problem is considered as an extended shortest path problem since we suppose that the best candidate path can minimize the criteria function.

It is assumed that a terrain map where a rover travels has been already given without any uncertainties. As shown in Fig. 2, the terrain map is represented as DEM (Digital Elevation Map) which is defined by a series of elevations along with a node n_i in (x_i, y_i, z_i) . Subscript i means a node number.

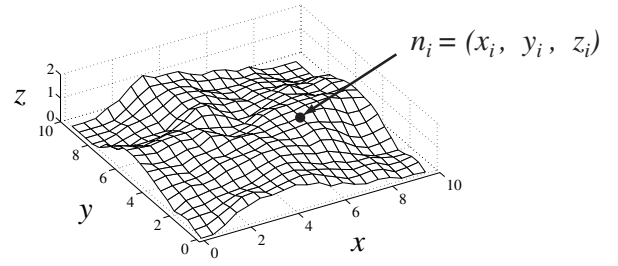


Fig. 2. Terrain map example (DEM: 50x50 nodes)

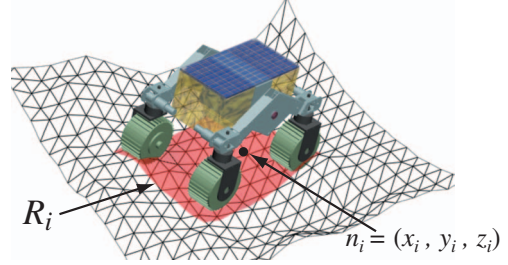


Fig. 3. Projection region of a rover on terrain

A. Criteria Index

The criteria function is composed of three indexes: terrain roughness, path length and terrain inclination.

1) *Terrain roughness index*: The terrain roughness index is employed in order to make the rover avoid uneven bumpy terrain. Also, this index implicitly indicates a chance of the wheel slippage since the traction load of the rover is not equally distributed to each wheel (then wheel slip will be caused) when the rover travels on uneven terrain.

Terrain roughness is defined based on the standard deviation of the terrain elevation over a projection region of a rover [6]. The projection region of the rover, denoted by R_i , is illustrated in Fig. 3. The region R_i includes the set of terrain elevation points inside the region surrounded by wheels as shown in Fig. 3.

Then, the terrain roughness index B_i is given as a standard deviation of the terrain elevation in the region R_i :

$$B_i = \sqrt{\frac{1}{n} \sum_{R_i} (z(R_i) - \bar{z}(R_i))^2} \quad (1)$$

where, n is a number of nodes inside the region R_i . $\bar{z}(R_i)$ is an average elevation in the R_i . The rougher the terrain is, the larger the value of B_i becomes.

2) *Path length index*: The path length index performs to find the shortest path form current position to a certain destination. The path length index L_i between adjacent nodes is simply calculated by the following equation:

$$L_i = |n_i - n_j| = \sqrt{(x_i - x_j)^2 + (y_i - y_j)^2 + (z_i - z_j)^2} \quad (2)$$

If the node n_j are not adjacent to the node n_i , L_i takes large enough value.

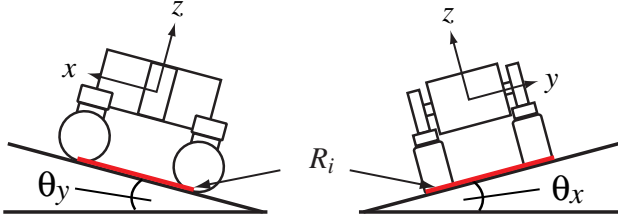


Fig. 4. Terrain inclination angles

3) *Terrain inclination index*: When a rover climbs up or traverses a slope, risks of wheel slippage or vehicle tip over become large since the traction load of the rover increases on the slope situation, as investigated in [12]. The index for the terrain inclination is applied to mitigate such risks. Terrain inclination angles are divided into two axes as described in Fig. 4. An inclination angle around x-axis of the rover coordinate is denoted by θ_x , while the one around y-axis is θ_y . The indexes, Θ_{x_i} and Θ_{y_i} , associated with each terrain inclination are respectively determined by the average inclination at the region R_i .

$$\Theta_{x_i} = \bar{\theta}_x(R_i), \quad (3)$$

$$\Theta_{y_i} = \bar{\theta}_y(R_i). \quad (4)$$

The index for the terrain inclinations also indicates a hazard for vehicle tip-over since the roll and pitch angle of the vehicle are assumed to be equivalent to the terrain inclination.

B. Criteria Function for Candidate Path

Using the above indexes, the criteria function $C(\mathbf{p})$ to find a candidate path \mathbf{p} is defined as follows:

$$C(\mathbf{p}) = \sum_{i=\mathbf{p}} \{W_B N_B B_i + W_L N_L L_i + W_{\theta_x} N_{\theta_x} \Theta_{x_i} + W_{\theta_y} N_{\theta_y} \Theta_{y_i}\} \quad (5)$$

where, W_B , W_L , W_{θ_x} and W_{θ_y} are weighting factors to give specific priorities between terrain roughness, path length and terrain inclinations. Note that, W_{θ_x} or W_{θ_y} respectively take large enough values when the index Θ_{x_i} or Θ_{y_i} exceed threshold angles, $\theta_{x_{max}}$ and $\theta_{y_{max}}$.

N_B , N_L , N_{θ_x} and N_{θ_y} are constant to make each corresponding index normalize and eliminate the dimensions. The path \mathbf{p} consists of a series of neighboring nodes, $\mathbf{p} = \{n_{start}, \dots, n_i, \dots, n_{goal}\}$.

The smaller each value of the index is, the less the hazard at the path is. Then, supposing the criteria function as a hypothetical distance function, the path-planning problem is equivalent to the shortest path search problem. Considering that the minimum criteria function derives the ‘‘shortest’’ path \mathbf{p}_s , the following equation can be formed:

$$\min C(\mathbf{p}) = C(\mathbf{p}_s). \quad (6)$$

To derive the path \mathbf{p}_s , the conventional Dijkstra’s algorithm is employed [7].

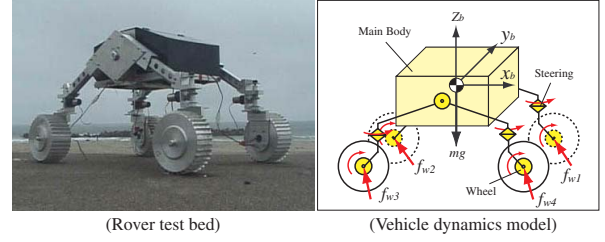


Fig. 5. Rover test bed and vehicle dynamics model

IV. DYNAMICS SIMULATION MODEL FOR PATH EVALUATION

To perform the dynamics simulation of path following, the dynamics simulation model is developed. In the simulation, the dynamic behavior of a rover is modeled with a wheel-and-vehicle model, which consists of two models: the vehicle dynamics model and the wheel-soil contact model. The interaction of wheel on loose soil is properly addressed based on the terramechanics approach. The wheel-and-vehicle dynamics model has been successfully developed and validated in our previous researches [10][11].

A. Vehicle Dynamics Model

In this research, the vehicle in the simulation is referred to our rover test bed which was developed by the authors, as shown in Fig. 5. The 4-wheeled rover test bed weighs about 35 [kg] in total. The rover has 0.48 [m] in the wheelbase and 0.34 [m] in tread. Each wheel of the rover has an active steering DOF. The vehicle dynamics model, illustrated in Fig. 5, has to be completely equivalent to the rover test bed. The dynamic motion equation of the vehicle is generally written as:

$$\mathbf{H} \begin{bmatrix} \dot{\mathbf{v}}_0 \\ \dot{\boldsymbol{\omega}}_0 \\ \dot{\mathbf{q}} \end{bmatrix} + \mathbf{C} + \mathbf{G} = \begin{bmatrix} \mathbf{F}_0 \\ \mathbf{N}_0 \\ \boldsymbol{\tau} \end{bmatrix} + \mathbf{J}^T \begin{bmatrix} \mathbf{F}_e \\ \mathbf{N}_e \end{bmatrix} \quad (7)$$

where the symbols used in the above equation are listed as:

- \mathbf{H} : inertia matrix of the vehicle.
- \mathbf{C} : velocity depending term.
- \mathbf{G} : gravity term.
- $\mathbf{v}_0, \boldsymbol{\omega}_0$: linear and angular velocity of the main body.
- \mathbf{q} : angle of each joint of the vehicle.
- \mathbf{F}_0 : forces acting at the main body.
- \mathbf{N}_0 : torques acting at the main body.
- $\boldsymbol{\tau}$: torques acting at each joint of the vehicle.
- \mathbf{J} : Jacobian matrix.
- $\mathbf{F}_e = [\mathbf{f}_{w1}, \dots, \mathbf{f}_{wm}]$: external forces acting at each wheel (m is the number of wheels.)
- \mathbf{N}_e : torques acting at each wheel

Note that, each external force \mathbf{f}_{wi} is derived by the wheel-soil contact model, as mentioned in (10)-(12) later. Here, the subscript i denotes the wheel number (in this case, $i=1 \dots 4$).

Equation (7) is general and can be applied to a vehicle with any configurations. Specific parameters for the rover

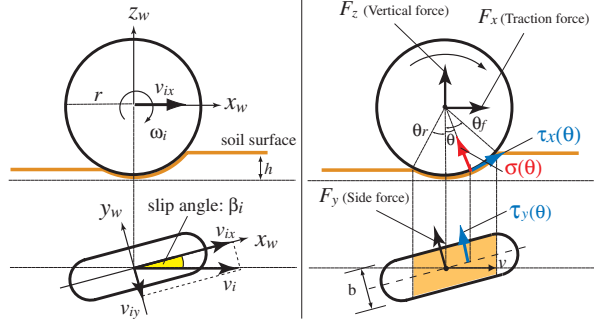


Fig. 6. Wheel-soil contact model

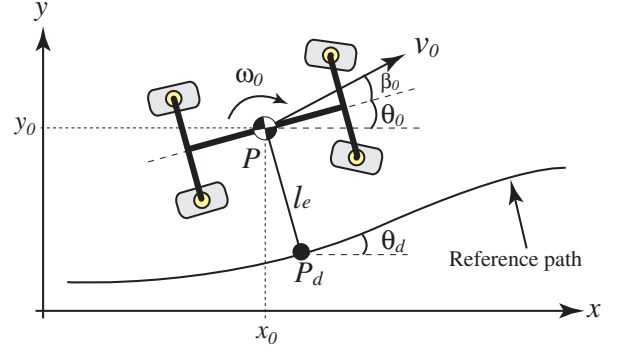


Fig. 7. Illustration of path following control

kinematics and dynamics are identified from the test bed and used in the simulation. The motion of the rover with given traveling and steering conditions is numerically calculated by solving (7) successively.

B. Wheel-Soil Contact Model

A general force model for a rigid wheel traveling on loose soil is presented in Fig. 6. The wheel coordinate system is defined as a right-hand frame as shown in Fig. 6, where the longitudinal direction is denoted by x_w , the lateral direction by y_w , and the vertical direction by z_w .

Wheel slip dynamics can be measured by *slip ratio* and *slip angle*. The slip in the longitudinal direction is defined as *slip ratio* s_i , which is calculated as a function of the longitudinal linear velocity v_{ix} and the circumference velocity of a wheel $r\omega_i$:

$$s_i = \begin{cases} (r\omega_i - v_{ix})/r\omega_i & (r\omega_i > v_{ix} : \text{driving}), \\ (r\omega_i - v_{ix})/v_{ix} & (r\omega_i < v_{ix} : \text{braking}) \end{cases} \quad (8)$$

where, r is a wheel radius. The slip ratio takes a value between -1.0 and 1.0 .

On the other hand, the slip in the lateral direction is measured by slip angle β_i , which is defined by the longitudinal and lateral linear velocities, v_{ix} and v_{iy} , of the wheel as follows:

$$\beta_i = \tan^{-1}(v_{iy}/v_{ix}). \quad (9)$$

Based on the terramechanics approach, wheel contact forces, such as a drawbar pull F_x , a side force F_y and a vertical force F_z , are able to obtain in the same fashion [8][9][10]:

$$F_x = rb \int_{\theta_r}^{\theta_f} \{\tau_x(\theta) \cos \theta - \sigma(\theta) \sin \theta\} d\theta, \quad (10)$$

$$F_y = \int_{\theta_r}^{\theta_f} \{rb \cdot \tau_y(\theta) + R_b \cdot (r - h(\theta) \cos \theta)\} d\theta, \quad (11)$$

$$F_z = rb \int_{\theta_r}^{\theta_f} \{\tau_x(\theta) \sin \theta + \sigma(\theta) \cos \theta\} d\theta \quad (12)$$

where, b is a width of the wheel, and $\sigma(\theta)$ is the normal stress underneath the wheel. $\tau_x(\theta)$ and $\tau_y(\theta)$ mean shear stresses in the longitudinal and lateral direction of the wheel. Also, the contact region of the wheel on loose soil is determined

by the entry angle θ_f and the exit angle θ_r . In addition, R_b is modeled as a reaction resistance generated by the bulldozing phenomenon on a side face of the wheel [10]. R_b is given as a function of a wheel sinkage h .

Note that, σ , τ_x and τ_y are key components to derive the wheel forces, and, they are dominated by wheel slippage. The contact region of the wheel is also depended on slip behaviors. Thus, the wheel-soil contact model can deal with the slipping wheel. The contact model has been successfully verified in [10].

V. PATH FOLLOWING STRATEGY

Path following strategy is shortly described to make the rover travel along with the planned path. The strategy is referred to our previous research in [13] which takes into account slip motions. According to the strategy, both steering and driving maneuvers of the rover are derived not only to follow an arbitrary path but also simultaneously compensate for the slip.

A. Path Following Control

A general illustration of the path following problem is shown in Fig. 7. The current vehicle's position is denoted by P , the shortest distance projection of P to a planned path is denoted by P_d . Each symbol used in the path following problem is defined as follows:

- l_e : signed distance between P and P_d (distance error.)
- θ_d : angle between the x-axis and the tangent to the path at P_d (vehicle's desired orientation.)
- θ_e : orientation error ($= \theta_0 - \theta_d$)
- β_0 : sideslip of the vehicle

In the path following problem, a feedback control law is employed to satisfy both $l_e \rightarrow 0$ and $\theta_e \rightarrow 0$. Then, the control objectives are realized by the use of one control variable, which is a turning angular velocity of the vehicle $\omega_0 (= \dot{\theta}_0)$. Thus, considering a linear state feedback control when v_0 (linear velocity of the vehicle) is constant and not be zero, a path following control input u_p is given by:

$$u_p = -k_1 v_0 l_e - k_2 |v_0| \theta_e - k_3 |v_0| \dot{\theta}_e \quad (13)$$

where, k_1 , k_2 and k_3 are control gains.

B. Sideslip Control

On loose soil, a vehicle has a certain amount of sideslip. It is simply deduced that the sideslip phenomenon must lead to an unexpected orientation error in the path following issue. Therefore, we consider that the sideslip can be reduced by another control objective, namely $\beta_0 \rightarrow 0$. Combining with the control input u_p represented in (13), another control input u_β , which decreases the sideslip, is modeled as:

$$u_\beta = k_4\beta_0 + k_5\omega_0 \quad (14)$$

where, k_4 and k_5 are control gains.

Note that these two control inputs, u_p and u_β , are selectively distributed to both steering and driving axles: for example, front wheel pair is controlled to follow a path by u_p , while rear pair compensates a sideslip by u_β .

C. Steering and Driving Maneuvers with Slip Compensation

The control inputs have to be distributed into several actuators that are mainly located on steering and driving units.

1) *Steering maneuvers*: A desired steering angle of each wheel δ_{di} is elaborated by the following equation:

$$\delta_{di} = \tan^{-1} \left[\frac{\dot{y}_d - \dot{Y}_i(\dot{\theta}_d)}{\dot{x}_d - \dot{X}_i(\dot{\theta}_d)} \right] - \theta_d - \beta_i \quad (15)$$

where, \dot{x}_d and \dot{y}_d are desired linear velocities to each direction. X_i and Y_i , derived by geometric constraints of the vehicle, are distances between every wheel and the center of gravity of the vehicle. \dot{X}_i and \dot{Y}_i become a function of $\dot{\theta}_d$, which is desired turning angular velocity of vehicle.

Then, desired control inputs to (15) are eventually summarized as follows:

$$[\dot{x}_d \ \dot{y}_d \ \dot{\theta}_d]^T = [v_d \cos \theta_d \ v_d \sin \theta_d \ u_p \ (\text{or } u_\beta)]^T \quad (16)$$

where, v_d is a desired linear velocity of the vehicle. Note that, the desired velocity v_d is chosen to be in inverse proportion to the path curvature on P_d .

2) *Driving maneuvers*: The driving maneuver is defined as a control of wheel angular velocity. A desired wheel angular velocity ω_{di} is derived as:

$$\omega_{di} = \begin{cases} \{ \dot{x}_d + \dot{X}_i(\dot{\theta}_d) \} \cdot \cos \beta_i / r \cos \phi_i & (\theta_d \leq \pi/4), \\ \{ \dot{y}_d + \dot{Y}_i(\dot{\theta}_d) \} \cdot \cos \beta_i / r \sin \phi_i & (\theta_d \geq \pi/4). \end{cases} \quad (17)$$

Additionally, the desired wheel angular velocity has to be adjusted to compensate the longitudinal slip of wheel. Then, an improved desired angular velocity $\hat{\omega}_{di}$ compensating the longitudinal slip is rewritten as follows:

$$\hat{\omega}_{di} = \omega_{di} / (1 - (s_{ref} - s_i)) \quad (18)$$

where, s_{ref} means a reference slip ratio to regulate the longitudinal slip of a wheel. In our approach, the value of s_{ref} is given between 0.1 and 0.3, where a wheel traction is obtained the most efficient value referring to our previous researches.

VI. SIMULATION OF PATH PLANNING AND EVALUATION

In this section, the simulation study and the performance of the proposed technique are described. The path planning and evaluation simulation was conducted along with comparisons of two candidate paths. Each path is evaluated based on wheel slippage, vehicle postures and elapsed time/total traveling distance to reach a certain destination.

A. Simulation procedure

The path planning and evaluation simulation is executed as follows:

- 1) Input terrain elevation map to the path planning algorithm.
- 2) Input weighting factors and thresholds for terrain inclinations into (5).
- 3) Find the candidate path p_s from the initial to the destination based on (6).
- 4) The planned path is plugged into the dynamics simulation of path following.
- 5) Derive the path following control inputs u_p and u_β using (13) and (14).
- 6) Calculate the desired steering angles δ_{di} and angular velocities $\hat{\omega}_{di}$ based on (15) and (18).
- 7) Calculate the external forces f_{wi} acting to each wheel using the wheel-soil contact model ((10)-(12)).
- 8) Determine F_0 , N_0 , F_e , N_e and τ .
- 9) Solve (7), then obtain the rover position, orientation and velocities.
- 10) Calculate the sideslip of the rover, slip ratios and slip angles of each wheel, then return to the step 5) until the rover arrives at the destination.
- 11) Finally, the path is evaluated based on the motion profile obtained by the dynamics simulation.

B. Terrain Elevation Map

As shown in Fig. 8, the terrain elevation map is 8 [m] \times 8 [m] square with a grid of 50 \times 50 equally-spaced terrain nodes (total nodes in the map are 2500.) The elevation map is obtained by the fractal method as presented in [14]. In the simulation, the surface is supposed to be evenly covered with the *Lunar Regolith Simulant*, which is simulated lunar surface soil in terms of similar material components and mechanical characteristics [15]. The wheel-soil contact model is used the soil specific parameters of the Lunar Regolith Simulant.

C. Path Planning and Discussion

We carried out the simulation along with two candidate paths, Path-A and Path-B, generated by changing thresholds for terrain inclinations Weighting factors and the thresholds to find these two paths are summarized in Table I.

The planned paths are depicted in Fig. 8. The path characteristics values, such as total length and inclinations of the path, are summarized in Table II. It can be seen that the Path-A is generated as making the path directly connect from the start to the goal, while the Path-B is planned to avoid a hill located around the center of the map. The

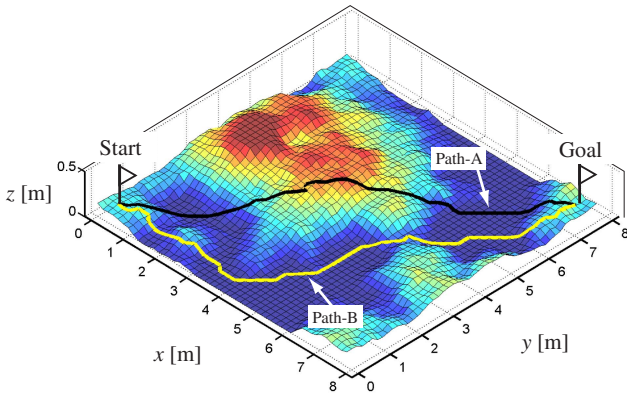


Fig. 8. Illustration of terrain elevation map and planned paths

TABLE I
WEIGHTING FACTORS AND THRESHOLDS

Path	W_B	W_D	W_{θ_x}	W_{θ_y}	$\theta_{x,max}$ [deg]	$\theta_{y,max}$ [deg]
Path-A	0.3	0.3	0.2	0.2	15.0	15.0
Path-B	0.3	0.3	0.2	0.2	7.5	7.5

threshold for terrain inclinations explains this difference. The characteristics of each path can be deduced as follows: the Path-A is relatively short path, but implies hazards of wheel slippage or vehicle instability. The Path-B is expected to be a hazard less path, but it will take longer time to reach the goal.

D. Path Evaluation and Discussion

As described above, two paths are evaluated using motion profiles obtained by the dynamics simulations.

Time profiles of vehicle orientations (roll and pitch angles), slip ratios and slip angles of each wheel are shown in Fig. 9, Fig. 10 and Fig. 11, respectively. Fig. 12 illustrates the dynamic motion of the rover on each planned path. Path evaluation results focused on the elapsed time, slip ratio, and slip angle are listed in Table III. Here, the values of the slip ratio and slip angle are respectively evaluated by employing RMS (Root Mean Square).

According to the figures and the table, first, it can be

TABLE II
CHARACTERISTICS OF PLANNED PATHS

Path	Total length [m]	Inclinations [deg]			
		Maximum		Deviation	
		θ_x	θ_y	θ_x	θ_y
Path-A	10.60	12.37	9.67	5.17	4.26
Path-B	12.42	5.93	7.49	2.34	2.63

TABLE III
PATH EVALUATION RESULTS

Path	Elapsed time [sec]	Slip ratio (RMS)	Slip angle (RMS) [deg]
Path-A	175.0	0.08	2.37
Path-B	197.5	0.08	1.19

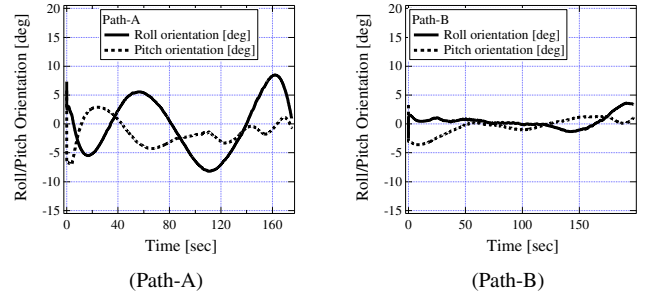


Fig. 9. Simulation result : time profile of vehicle orientation

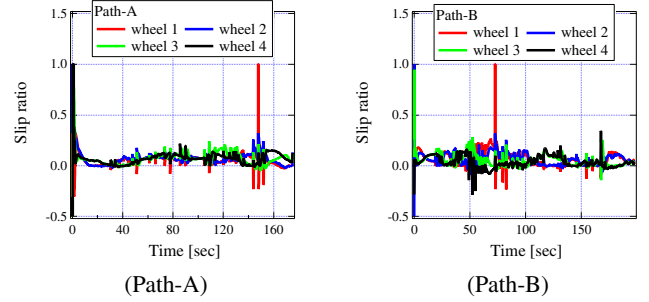


Fig. 10. Simulation result : time profile of slip ratio

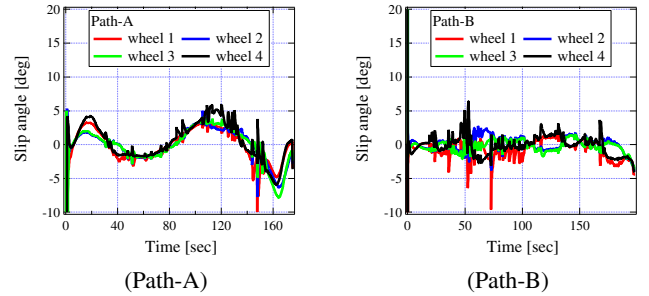


Fig. 11. Simulation result : time profile of slip angle

clearly seen that the vehicle orientation on Path-A has more fluctuation (around ± 10 [deg]) than the one on Path-B since the terrain inclination on Path-A is rougher than the one on Path-B. This result indicates that Path-A might have a hazard in tip over or wheel slippage.

Interestingly, however, there are few differences in slip ratio of wheels on both paths. The result in slip ratio conflicts with the one in the vehicle orientation. This is probably due to the path following control with slip compensation.

According to Fig. 11 and Table III, the deviation of slip angle on Path-A is almost twice as large as the that of Path-B. This can be explained that the large slip angle, which is observed from 80 [sec] to 120 [sec] in Fig. 12 and Fig. 11, is caused by the hill placed around the center of the map.

VII. CONCLUSION AND FUTURE WORKS

In this paper, the path planning and its evaluation method for lunar/planetary exploration rovers has been addressed with paying attention to wheel slip dynamics. The proposed technique is composed of three steps; 1) path planning to find

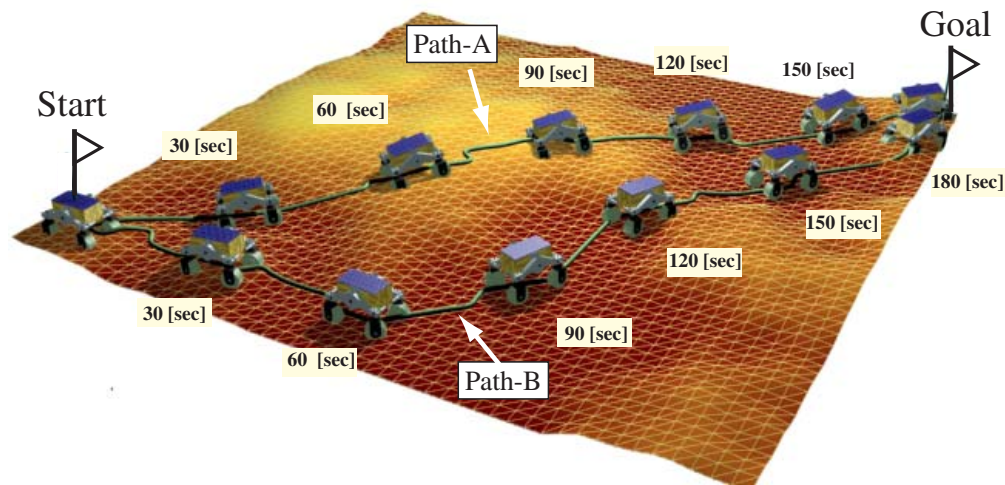


Fig. 12. Illustration of path evaluation simulation

a candidate path, 2) dynamics simulation with path following to the planned path, and 3) path evaluation based on the dynamic simulation results.

The demonstration of the proposed technique was presented through a comparison between two different paths. The result shows that the proposed technique is able to quantitatively evaluate and discuss which path are slip less, hazard less, and the safest. It is expected that the optimal motion planning for a rover can be derived by recursively conducting the proposed technique.

In the step of the path planning, the weighting factors were given constant values, however, to find more reasonable path, it will be necessary to dynamically adjust these values based on vehicle/terrain situations. In addition, since the surface of the planetary body consists of soft soil and hard rocks/stones, the terrain characteristics, such as soil parameters (soil cohesion stress or soil friction angle) should be included in the path planning approach.

REFERENCES

[1] <http://marsrovers.jpl.nasa.gov/home/index.html> (as of February 2006)
 [2] A. De Luca, G. Oriolo and C. Samson; *Robot Motion Planning and Control*, edited by J.-P. Laumond, Springer-Verlag, 1998.
 [3] Z. Shiller and Y. R. Gwo; "Dynamic Motion Planning of Autonomous Vehicles," *IEEE Transaction on Robotics And Automation*, vol. 7, no. 2, pp. 241-249, April 1991.
 [4] T. Kubota, Y. Kuroda, Y. Kunii and T. Yoshimitsu; "Path Planning for Newly Developed Microrover," *Proc of the 2001 IEEE Int. Conf. on Robotics And Automation*, pp. 3710-3715, 2001.
 [5] T. M. Howard and A. Kelly; "Terrain-Adaptive Generation of Optimal Continuous Trajectories for Mobile Robots," *Proc. of the 8th Int. Symp. on Artificial Intelligence, Robotics and Automation in Space*, 2005.
 [6] K. Iagnemma and S. Dubowsky; *Mobile Robot in Rough Terrain*, Springer Tracts in Advanced Robotics, vol.12, 2004.
 [7] Steven M. LaValle; *PLANNING ALGORITHMS*, Cambridge University Press, 2006.
 [8] M. G. Bekker; *Introduction to Terrain-Vehicle Systems*, The University of Michigan Press, 1969.
 [9] J. Y. Wong; *Theory of Ground Vehicles*, John Wiley & Sons, 1978.
 [10] G. Ishigami and K. Yoshida; "Steering Characteristics of an Exploration Rover on Loose Soil Based on All-Wheel Dynamics Model," *Proc of the 2005 IEEE Int. Conf. on Intelligent Robots and Systems*, pp. 2041-2046, 2005.

[11] G. Ishigami, A. Miwa and K. Yoshida; "Steering Trajectory Analysis of Planetary Exploration Rovers Based on All-Wheel Dynamics Model," *Proc. of the 8th Int. Symp. on Artificial Intelligence, Robotics and Automation in Space*, 2005.
 [12] G. Ishigami, A. Miwa, K. Nagatani and K. Yoshida; "Terramechanics-Based Analysis on Slope Traversability for a Planetary Exploration Rover," *Proc. of The 25th Int. Symp. on Space Technology and Science*, 2006.
 [13] G. Ishigami, K. Nagatani and K. Yoshida; "Path Following Control with Slip Compensation on Loose Soil for Exploration Rover," *Proc of the 2006 IEEE Int. Conf. on Intelligent Robots and Systems*, (will be published) 2006.
 [14] Y. Yokokoji, S. Chaen and T. Yoshikawa; "Evaluation of Traversability of Wheeled Mobile Robots on Uneven Terrains by Fractal Terrain Model," *Proc of the 2004 IEEE Int. Conf. on Robotics And Automation*, pp. 2183-2188, 2004.
 [15] G. Heiken, D. Vaniman, B. M. French and J. Schmitt; *Lunar Sourcebook: A User's Guide to the Moon* Cambridge University Press, 1991.